# Performance of source imaging techniques of spatially extended generators of uterine activity

S. Zahran, A. Diab, R.A. Chowdhury, T. Hedrich, M. Hassan, C. Grova, M. Yochum, M. Khalil, Catherine Marque

Informatics in Medicine Unlocked 16 (2019) 100167

Contents lists available at ScienceDirect

Informatics in Medicine Unlocked

journal homepage: www.elsevier.com/locate/imu

# Performance of source imaging techniques of spatially extended generators of uterine activity

Saeed Zahran[a,b,f,d,*], Ahmad Diab[e], Rasheda Arman Chowdhury[c], Tanguy Hedrich[c], Mahmoud Hassan[d], Christophe Grova[c,g], Maxime Yochum[d], Mohamad Khalil[b,f], Catherine Marque[a]

[a] Sorbonne University, Université de technologie de Compiègne, CNRS, UMR 7338 BMBI, 60200, Compiègne, France
[b] Facuty of Engineering, Lebanese University, Lebanon
[c] Multimodal Functional Imaging Lab, Biomedical Engineering Department, McGill University, Montreal, Quebec, Canada
[d] U1099 INSERM, Laboratoire Traitement du Signal et de l'Image LTSI, Université de Rennes 1, France
[e] Faculty of Public Health, Lebanese University, Lebanon
[f] AZM Centre for Research in Biotechnology at the Lebanese University, Lebanon
[g] Physics Department and PERFORM Centre, Concordia University, Montreal, Canada

ARTICLE INFO

*Keywords:*
EHG
Uterine activity
Source imaging

ABSTRACT

Preterm birth (PTB) is one of the most important complications in pregnancy. Reliable diagnosis means are lacking and the underlying physiological mechanisms are unclear. Determining the location of various correlated and simultaneously active uterus sources from abdominal ElectroHysterogram (EHG) recordings and extracting the corresponding uterus signals is a challenging problem. The use of the EHG for imaging the sources of the uterine electrical activity could be a new and powerful diagnosis technique. In this paper we compare the ability of six distributed source localization methods to recover extended sources of uterus activity from abdominal EHG. As no gold standard to evaluate source localization methods, exists, we perform our evaluation by using a well-controlled realistic simulations of EHG signals, involving several locations. Simulated data were corrupted by physiological EHG noise. The performance of several state-of-the-art techniques for extended source localization is evaluated using a detection accuracy index using the Dipole Localization Error, the Area Under the Receiver Operating Characteristic (ROC) Curve AUC, and the Correlation Coefficient.

## 1. Introduction

Uterine contractility is a straightforward consequence of the underlying electrical activity in the myometrial cells [1]. The electrical activity of the uterus is one of the most promising tools for the detection of preterm labor signs [2–4]. Electrohysterography (EHG) measures uterine electrical activity (Uterine electromyogram, uEMG) generated by the underlying activity in the myometrial cells using a few number of sensors uniformly distributed on the mothers abdominal skin [5]. It is a long-standing technique for the analysis of uterine activity. Due to its good temporal resolution, the EHG is used to monitor uterine contraction and has proven to be useful in the clinical evaluation of uterine activity as early as 18 weeks of pregnancy [6–11]. It have been more recently used as a noninvasive technique to identify uterus activation patterns, which plays a crucial role as it is the only technique with the Magnetomyography (MMG) providing information directly linked to the generation of the uterine activity. Performing an accurate localization of EHG sources is thus of particular interest leading to recognize their generation and propagation. One of the most recent processing techniques introduced is the imaging of the source of the electrical activity based on source localization from the EHGs [12–16]. This technique allows a noninvasive reconstruction of the electrical potential on the uterine surface based on electrical potential measurement on the body surface and anatomical data related to the abdominal conducting volume. This non-invasive modality is used in this study to localize uterus regions involved during the generation of burst of contractile activity. Uterine activity originates from excitability and synchronization of myometrial cells. This synchronization could be the result of two phenomena: a) raised connectivity in the myometrial cells, due to the appearance of Gap Junctions, which results in an increase in the local diffusion of the action potentials [5]; b) increased sensitivity to mechanotransduction, at the cell level, that permits a longer distance

* Corresponding author. Sorbonne University, Université de technologie de Compiègne, CNRS, UMR 7338 BMBI, 60200, Compiègne, France.
*E-mail address:* saeed.zahan@inserm.fr (S. Zahran).

https://doi.org/10.1016/j.imu.2019.100167
Received 26 October 2018; Received in revised form 5 March 2019; Accepted 7 March 2019
Available online 11 September 2019

activation of the uterine muscle due to its stretching [17]. Caldeyro-Barcia described their model of uterine function as a wave-like contraction which starts at the fundus, spreads down the uterus, and decreases in strength and duration as it progresses [18]. Wolfs and van Leeuwen [19] estimated a linear propagation. However, there is a significant doubt that myometrial action potentials travel in straight paths. Furthermore the amplitude of Magnetomyography (MMG) signals for physiological uterine activity is expected to range from pico ($10^{-12}$) to femto ($10^{-15}$) Tesla (T), depending on the approach of measurement [20]. As mentioned in Ref. [21]; uterine burst activity give rise to a relatively large amplitude (4.5 pT). This implies that MMG signals are likely to arise from large spatially extended regions of active uterus. Thus uEMG are detectable on EHG/MMG recordings only when associated with a spatially extended uterus generator of several square centimeters. Therefore it is necessary to rate the capacity of source localization methods to recover such spatial extent of the sources. Therefore, not only it is important to localize the origin of uEMG but also to recover their spatial extent and estimate the temporal course of their activity. This task can become particularly challenging when several distributed regions with highly synchronized activity are simultaneously active or are involved during a propagation process. Source localization methods may facilitate to define the regions of the uterus where the activity are generated [13]. Studying the underlying mechanisms and anatomical areas involved in the generation and the propagation of uEMG constitutes a key issue toward a better understanding of the uterus. This method is mostly referred to source imaging and permits to identify the uterus regions that are involved in generating characteristic activity patterns, which is of clinical relevance. Inferring the source location within the uterus from a signal acquired on the abdominal skin, i.e., the EHG inverse problem, is an ill-posed problem since there is a large number of source configurations that can turn out the same potential at the surface of the abdominal skin. Additional constraints should then be added to obtain a unique solution. Two types of approaches have been proposed [22,23]. (1) The equivalent current dipole methods assume that the potentials are generated by a few dipolar sources [24,25]. (2) The distributed source methods assume that surface potentials are generated by a large number of dipolar sources distributed within source space [26]. Distributed source methods seem appropriate to estimate spatially extended sources. They aim at localizing myocyte activation on a large number of sources (around 5000) given few sensors (around 64 or less). The problem is then highly underdetermined and requires additional constraints in the form of a regularization technique. In this study we add a priori knowledge or constraints by fixing the position of the sources along the uterus surface to achieve linearity in the inverse problem. However, the problem is still under-determined due to the small number of electrodes. In order to get a unique solution, further constraints in the form of a regularization are required. Some mathematical constraints were proposed, such as the solution with the minimum energy (Minimum Norm Estimate) [27] or The solution with the highest spatial smoothness [28]. Statistical frameworks, based on Bayesian inference [29] or entropy [30,31]; were proposed in the state of the art to provide a flexible way of introducing prior information. Abdominal EHG performance is limited as the uterus often demonstrates several simultaneously active regions and as EHGs present low signal-to-noise ratios. Indeed, this interpretation is not straightforward as signals are severely impacted by the effects of volume conduction. To overcome these difficulties, we need to make the analysis on the temporal dynamics of uterus sources reconstructed from surface EHG. Our objective here was to carefully compare different methods, to assess their detection accuracy when extended uterus areas were activated. To do so, we used a common ground-truth fully controlled simulation environment. This environment involves different patterns of source configurations in particular with respect to the number of sources, their spatial properties, and their level of synchronization. It also takes into account an equivalent number of channels, realistically shaped uterus model and simultaneous recordings. All simulated data were corrupted by averaged physiological EHG noise. Six source localization methods were evaluated and compared, namely: the Standardized low resolution brain electromagnetic tomography (sloreta) [32]; the Standard Maximum Entropy on the Mean (cMEM) [33]; STWV-DA and STF-DA [34]; the Sparse, variation-based source imaging approaches [35]. We quantified the performance of each method using the Dipole Localization Error, the Area Under the Receiver Operating Characteristic (ROC) Curve AUC, and the Correlation Coefficient. To overcome the accuracy issues when using Boundary Element solutions due to the high conductivity ratio between neighboring tissues (muscle/fat conductivity ratio), we solved the forward problem using Symmetric Boundary Element [36] which belong to the Green representation theorem [37]. Finally, we applied the source localization method to actual EHG recordings, where linear propagation of activity is not seen and the electrical propagation demonstrates complex patterns. Thus the action potentials are found to not travel linearly. The organization of this paper is as follows. First, we present the data model on which the examined methods are based, then, introduction of the source localization method is proposed, followed by the description of the realistic simulation dataset. Then, an explanation of the evaluation process and the performance criteria is given. Then the results, discussion and conclusion are provided.

## 2. Materials and methods

### 2.1. Data model

The electrical potential that can be seen at the surface of the abdominal skin originates mostly from myometrium cells that are primarily located in the middle layer of the uterine wall, consisting mainly of uterine smooth muscle cells (also called myocytes). In order to get a signal of appropriate amplitude to be measurable at the skin surface, a certain number of simultaneously active myocyte populations is required. We used in this study an electrical model of these populations developed by our team, based on an Hodgkin-Huxley approach. All details can be found in Ref. [38]. The variables of the electrical model are described by the following equations:

$$\frac{dV_m}{dt} = \frac{1}{C_m}(I_{stim} - I_{ca} - I_k - I_{kCa} - I_L) \tag{1}$$

$$\frac{dnk}{dt} = \frac{h_{k\infty - nk}}{\tau_{nk}} \tag{2}$$

$$\frac{d[Ca]^{2+}}{dt} = fc[-\alpha I_{Ca} - k_{Ca}[Ca^{2+}]_i] \tag{3}$$

where $Vm$ is the transmembrane potential, $n_K$ is the potassium activation variable, $k_{Ca}$ is the Calcium extraction factor and $[Ca^{2+}]_i$ the intracellular calcium concentration. The ionic currents are $I_{Ca}$ for the voltage dependent calcium channel current, $I_K$ for the voltage dependent potassium channel current, $I_{kCa}$ for the calcium dependent potassium channel current and $I_l$ for the leakage current. The electric potential at the surface of the skin is the summation of signals originating from all over the uterus. In our simulations, we define a source space made of $D$ dipoles located on the uterus surface with a fixed orientation perpendicular to the surface. More particularly, the dipoles are positioned at the vertex of the triangles of the mesh of the uterus surface. The shape of the uterus has been segmented from a standard 3D MR data set by the FEMONUM project [39] that offers the scientific community 3D fetal, uterine and abdominal triangulated meshes. The triangle vertices will later become the source locations. In the same fashion, the compartment borders of skin, fat, and muscle are segmented, subsampled, and triangulated. The lists of some hundred triangles serve as the geometric model for the Symmetric Boundary Element Method used in the forward calculations [40]. The EHG

measurements ($X \in \mathbb{R}t^{N\times T}$) recorded by N electrodes for T time samples, contain a linear mixture of the sources ($S \in R^{D\times T}$) in the presence of noise ($N \in R^{N\times T}$), such that:

$$X = GS + N \tag{4}$$

where ($G \in R^{N\times D}$) is the lead field matrix that represent the propagation in the volume conductor and depends on spatial parameters of the model, such as the geometry of the uterus, muscle, fat and abdominal skin as well as their conductivities, and $D$ denotes the number of dipoles. For a given model, a Symmetric Boundary Element Method [40] method is used to calculate the lead field matrix. To develop our algorithms, we further assume that the dipoles of the source space are located on the uterus surface with orientations perpendicular to this surface. The EHG inverse problem then consists in reconstructing the sources S based on the surface measurements X for a given lead field matrix G. However, as the number of dipoles (several thousands) generally exceeds the number of sensors (several tenths), this problem is ill-posed. In order to restore identifiability of the ill-posed linear inverse problem, further assumption concerning the sources have been made. We applied a spatial prewhitening step by the multiplication of the data and the lead field matrix with the prewhitening matrix $P = K^{+}$, where $K$ can be computed from the background activity thaking the square root of its covariance matrix. The goal of this pre-whitening is to decorrelate the source signals, in order to facilitate the separation of the components.

### 2.2. Source localization and extraction

In this work, we compared six different methods, to assess their detection accuracy when extended uterus areas were activated.

#### 2.2.1. Standardized low resolution brain electromagnetic tomography (sLORETA)

The idea of the conventional sLORETA algorithm [32] consists in standardizing the Minimum Norm Estimte (MNE) solution, by weighting the current dipoles estimated on a voxel grid. We adapted this method to our situation by replacing the voxel grid by a surface grid that considers only dipoles on the uterus surface with an orientation perpendicular to this surface [32].

$$\hat{D}_{sLORETA} = \hat{D}^{T}_{MNE,1}\left\{|V_{\hat{D}}|\right\}^{-1}\hat{D}_{MNE,1} \tag{5}$$

where $|V_{\hat{D}}|^{-1}$ defined as $G^{T}[GG^{T} + \lambda I]^{-1} \in R^{N_d\times N_r}$ is the Tikhonov-regularized inverse matrix of $G$ and $I$ stand for the identity matrix.

#### 2.2.2. Transform-based tensor methods

This transform-based tensor method has been used here, as a processimg step to reduce to reduce the noise on the lead field matrix when several extended sources are used. The 3-dimensional data tensor to be treated by the CP decomposition, can either be computed as a transform over time of the electric potential measurements, which leads to the Space-Time-Frequency (STF) analysis, or as transform over space, leading to Space-Time-Wave-Vector (STWV) data.

#### 2.2.3. Space-Time-Frequency (STF) analysis

This method utilized for the time-frequency analysis consists in employing the wavelet transform of the time signals $x(r, t)$ of the diverse channels [41]. The resulting three dimension data can then be stored into the data tensor. To decompose the tensor $W$ by using the CP decomposition, time and frequency are considered as separate variables, leading to a trilinear tensor.

$$\begin{aligned} W(r, t, f) &= \int_{-\infty}^{\infty} x(r, t)\Psi(\alpha, \tau, t)d\tau \\ &\approx \sum_{p=1}^{R} a(r_i, p)b(t_j; p)c(f_k; p). \end{aligned} \tag{6}$$

where $r_i, t_j$ and $f_k$ represent the space, time, and frequency variables and $a(r_i; p)$, $b(t_j; p)$, $c(f_k; p)$ the elements of the loading matrices $A$, $B$, and $C$ are the space, time, and frequency characteristics, respectively. The loading matrix $A$, that contains the spatial characteristics, gives a good estimate of the spatial mixing matrix $\hat{H}^{(e)}$. Pseudoinverse of the estimated spatial mixing matrix $\hat{H}^{(e)}$ is used to obtain an improved estimate of the signal matrix $\hat{S}^{(e)}$:

$$\hat{S}^{(e)} = \hat{H}^{(e)+}X \tag{7}$$

#### 2.2.4. Space-Time-Wave-Vector (STWV) analysis

Space-Time-Wave-Vector (STWV) is acquired by a Fourier transform over space accomplished on the measured data. The spatial Fourier transform is calculated within a certain region on the uterus, selected by the spherical window function $w(r'\text{-}r)$ centered at a sensor position r, the STWV tensor

$$\begin{aligned} F(r_k, t_l, k_m) &= \int_{-\infty}^{\infty} w(r' - r_k)x(r', t_l)e^{jk_m^{T}r'}dr' \\ &\approx \sum_{r=1}^{R} a_r(r_k)b_r(t_l)c_r(k_m). \end{aligned} \tag{8}$$

is obtained [42]; where variable $k_m$ is the wave vector which indicate the direction of the changes of electric potential. Here, $w(r' - r_k)$ is a window function that selects data to the sensor with position $r_k$ for the local transform and $a_r(r_k)$, $b_r(t_l)$, and $c_r(k_m)$, denote the space, time, and wave vector characteristics, which are obtained by the CP decomposition of the tensor. This analysis requires knowledge of the sensor positions, specified by the matrix r, and of the number of expected sources (corresponding to the number of CP components) R. The tensor is decomposed by using the DIAG algorithm [43,44]. The results of the tensor decomposition yield an estimate of the signal matrix $\hat{S} = [b_1, ..., b_R]$, describing the temporal dynamics of each source. An estimate of the so-called spatial mixing matrix $H = [h_1, ..., h_R]$, which characterizes the spatial distribution of each source at the sensor level, is obtained as $\hat{H}^{(e)} = X\hat{S}(e)+$, where $\hat{S}^{(e)+}$ denotes the pseudo-inverse of $\hat{S}^{(e)}$.

$$\hat{H}^{(e)} = X\hat{S}^{(e)+} \tag{9}$$

#### 2.2.5. Disk algorithm (DA)

We then used the Disk Algorithm to localize the extended sources from the estimated spatial mixing matrix obtained after the application of the STWV and STF methodes, [34]. The Disk Algorithm aims to recover preciselly the extended source by using small circular-shaped patches of dipoles, called the disks. The localization of the extended sources is done for each component separately by comparing the spatial mixing vectors $\hat{h}_r$, $r = [1, ..., R]$, estimated in the first step, to the spatial mixing vectors associated with a number of potential distributed sources contained in a dictionary. We used this DA, for patch localization, combined with the STF and STWV preprocessing steps. Depending on the used preprocessing method, we thus obtain two methods referred to as STF-DA and STWV-DA.

### 2.3. Variation-based

The variation-based algorithm [35] is a source imaging method based on structured sparsity, which improves the Variation-Based Sparse Cortical Current Density (VB-SCCD) method. More particularly, it imposes sparsity on the variational map and in the original source domain by solving the following optimization problem:

$$\|\mathbf{X} - \mathbf{GS}\|_{F}^{2} + \lambda(f(\mathbf{VS}) + \alpha f(\mathbf{S})) \tag{10}$$

where the regularizing function $f$ is either the $L_1$-norm (for SVB-SCCD) or the $L_{1,2}$-norm (for L1,2-SVBSCCD). VB-SCCD optimization problem assumes a piece-wise constant spatial source distribution, and can be regarded as a particular case of (10) where $\alpha = 0$.

### 2.4. Standard Maximum Entropy on the mean (cMEM)

The Maximum Entropy on the Mean solver is established on a probabilistic algorithm where deduction on the current source densities is estimated from the data. The central characteristic of this technique is its capacity to regain the spatial extent of the implied sources. Its solution is rated by returns the distribution of source densities to a point out distribution in which source densities are systematic into partitions displaying identical activation state. Furthermore a constraint of spatial smoothness in each partition can be introduced [33].

### 2.5. Evaluation

#### 2.5.1. Area Under the Receiver Operating Characteristic(ROC) curve, AUC

AUC was proposed in Ref. [45] as a detection precision index (between 0 and 1), to assess the sensitivity of a source localization method to the spatial extent of the underlying generator. An AUC value greater than 0.8 was considered a good detection accuracy. The AUC index is assessing towards a Ground Truth the normalized energy of a source map at a specific time sample.

#### 2.5.2. Dipole Localization Error (DLE)

The Distance of Localization Error (DLE) [46]; which describes, the variation between the original and the estimated source configurations, is defined as follows:

$$DLE = \frac{1}{2Q}\sum_{k\in I}\min_{l\in\hat{I}}\|r_k - r_l\| + \frac{1}{2\hat{Q}}\sum_{l\in\hat{I}}\min_{l\in\hat{I}}\|r_k - r_l\| \quad (11)$$

where $Q$ and $\hat{Q}$ are the numbers of original and estimated active dipoles i.e., $Q = \#I$, $\hat{Q} = \#\hat{I}$, and $r_k$ denotes the placement of the $k - th$ source dipole.

#### 2.5.3. Correlation coefficients

In order to analyze the quality of the extracted signals of the different methods, we compute the correlation coefficients between the original and the estimated signals of the uterine activity components. The quality of the extracted sources is evaluated by calculating this correlation coefficients between the estimated patch signal and the averaged signal of all dipoles pertinence to a patch. We then calculate the mean of the correlation coefficients for all patches.

## 3. Results

We compare the performance of SVB-SCCD, VB-SCCD, STWV-DA, STF-DA, cMEM and sLORETA based on computer simulations. To this end, EHG data are generated for N = 30 electrodes using a realistic uterus and abdomen model with four compartments that represent the uterus, the muscle, the fat and the skin. To generate the extended sources, a number of patches each of which consists of 20 adjacent dipoles was considered. Highly-correlated uEMG signals comprising 200 time samples with a sampling rate of 200 Hz are created for all dipoles of one patch. The central interest of the techniques consists in their capability to extract several simultaneously active patches. To study the influence of the patch distance on the source localization results, we consider in this study three configurations of two surface patches with different distances, amounting to approximately 15 cm, 10 cm, and 5 cm, respectively. This will permit us to test the spatial resolution of the methods. We used 2 patches with highly synchronized activities but delayed by a number of time samples depending on the distance between the two patches. Indeed, assuming that in the uterus, the different sources are activated due to a propagation of uEMG, the same signals for the dipoles was used for the second patch but introduce a delay. For small distances, a random delay of 5 ms is used for each signal. For medium distances the signals are shifted 13 ms and for large distances, a signal delay of 20 ms is employed. The performance accomplished with the different source imaging algorithms for the three scenarios, averaged over 20 realizations with different patch signals (by introducing small variations in amplitude and delay) and noise, is summarized in Tables 1 and 2. Fig. 1, shows the AUC boxplot obtained for the different source localization methods for both raw and prewhitened EHG data for the three scenarios (three configurations of patch), averaged over 20 realizations with different patch signals.

**Table 1**
Representation of source imaging methods in terms of DLE (in cm) and signal correlation for the considered scenarios with large patch distance (1), medium patch distance (2), and small patch distance (3), applied to raw EHG data.

| Scenario | DLE | | | Correlation coefficient % | | |
|---|---|---|---|---|---|---|
| | 1 | 2 | 3 | 1 | 2 | 3 |
| SVB-SCCD | 0.12 | 2.12 | 3.01 | 96.6 | 93.2 | 90.09 |
| VB-SCCD | 0.14 | 2.9 | 5.9 | 95.1 | 91.2 | 80.9 |
| cMEM | 4.2 | 5.34 | 6.3 | 75.3 | 73.4 | 72.3 |
| STWV-DA | 6.43 | 8.3 | 12.4 | 71.44 | 68.11 | 60 |
| STF-DA | 25.16 | 20.67 | 17.4 | 47.5 | 52.6 | 55.67 |
| sLORETA | 10.56 | 12.54 | 17.8 | 65.43 | 59.8 | 54.89 |

**Table 2**
Representation of source imaging methods in terms of DLE (in cm) and signal correlation for the considered scenarios with large patch distance (1), medium patch distance (2), and small patch distance (3), applied to spatially prewhitened EHG data.

| Scenario | DLE | | | Correlation coefficient % | | |
|---|---|---|---|---|---|---|
| | 1 | 2 | 3 | 1 | 2 | 3 |
| SVB-SCCD | 0.98 | 1.4 | 2.59 | 97.65 | 95.41 | 92.5 |
| VB-SCCD | 0.99 | 1.9 | 3.2 | 96.4 | 94.7 | 90.52 |
| cMEM | 3.4 | 4.01 | 4.55 | 85.4 | 83.34 | 81.6 |
| STWV-DA | 3.3 | 4.23 | 4.7 | 85.7 | 83.23 | 81.17 |
| STF-DA | 13.16 | 12.67 | 10.15 | 56.9 | 59.4 | 65.88 |
| sLORETA | 5.67 | 8.9 | 11.12 | 76.45 | 75.6 | 72.42 |

When the source imaging algorithms are applied to the raw EHG recordings, for all three patch configurations, the AUC boxplot, the DLE and the correlation coefficient values show that both VB-SCCD and SVB-SCCD clearly outperform all other extended source localization approaches. For two patches (scenario 3), one can observe that SVB-SCCD approach clearly leads to better results than VB-SCCD. The SVB-SCCD method gives a superior separation of the sources than the VB-SCCD approach. cMEM and STWV-DA achieves comparable performances for all three source configurations. They does not permit to recover the patches as accurately as variation-based source imaging methods but perform better than sLORETA. STF-DA exhibiting high DLEs. The localization accuracy diminishes with decreasing source distance. The application of the source imaging algorithms to the prewhitened data improves the performance for all methods. In particular, the cMEM reaches the same performance as STWV-DA. STF-DA permits to recover both patches. Furthermore, the AUC results presented for each distance are comparable, indicating that the patch distance does not influence the source localization performance when using a prewhitened step for the data.

In Fig. 2 we applied the best method (SVB-SCCD) obtained from results in Table 1, Table 2 and Fig. 1 to real EHG signals in order to estimate the electrical activity on the surface of myometrium and how they are propagating in successive time windows. We used a standard protocol, to record the electrical activity of the uterine muscle. This protocol uses a grid of 16 monopolar electrodes (4 × 4 matrix) placed on the woman's abdominal skin, with two reference electrodes on each of her hips. The standardized system uses Ag/AgCl electrodes (8 mm diameter, with 17.5 mm distance between the centers of two adjacent electrodes). Each window in Fig. 2 represents 20 s of averaged data overlaps with the previous and subsequent windows by 10 s. Fig. 2

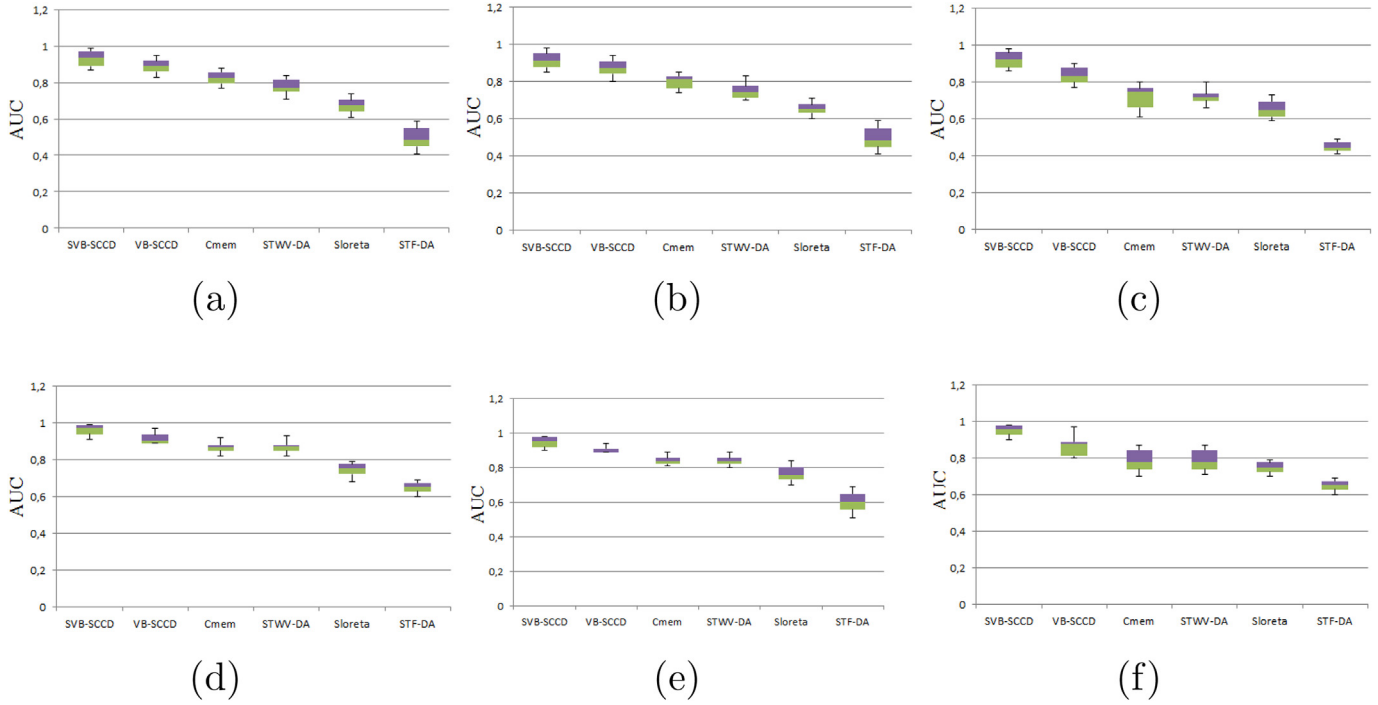


**Fig. 1.** AUC obtained for different methods applied to raw EHG data (up) and to spatially prewhitened EHG data (down) for three different scenarios composed of two patches with large distance (left), patches with medium distance (center), and patches small distance (right).

evidence the presence of hot spots of myometrial activity. Islands of activity appear without activation of neighboring muscle.

## 4. Discussion

A number of studies performed at the level of electrodes reported that electrohysterogram (EHG) associated with appropriate signal processing techniques might bring relevant information about normal networks activated. Indeed, this problem is complex due to the effects of volume conduction. In this paper we tackle this problem to overcome these difficulties, by working on the temporal dynamics of uterus sources reconstructed from surface EHG. We have conducted our analysis using a realistic uterus model and have aimed at recognizing the spatial extent of the sources. The computer simulations have shown that both SVB-SCCD and VB-SCCD exhibited the best performance, which permits to simultaneously localize several highly correlated active source regions as also shown in Ref. [13]. They appear therefore to be of the most promising approaches for the identification of multiple active uterus regions in the case of propagation. The SVB-SCCD technique allow to get further focal source estimates than VB-SCCD and realize the separation of even nearer sources, which leads to better performance in terms of signal extraction, due to the supplemental regularization term that assess sparsity in the original source. We have also analyzed the use of tensor-based methods which separate the sources prior to the localization. STWV method accurately separated the patches and exhibited good performance as also shown in Ref. [14]. This can be demonstrated by the fact that the STWV analysis correctly break the spatial mixing vectors of the two patches and therefore allows to localize each patch individually. The STWV-DA has proven to be robust if applied to the raw EHG data with no prewhitening, contrary to the other examined source imaging methods, with patches of medium and small distances, only lead to useful results in the case of prewhitened data. However, the tensor-based methods do not provide accurate results for the correlated sources in case of the STF analysis due to the highly correlated signals of the two patches that in this case differ by a short time delay due to the propagation of the activity [14,34]. The STF method does not permit in that situation to separate the sources, therefore impeding a correct source localization. This poor sensitivity may be explained by the fact that the STF analysis is unable to separate the different patches activities, because their time-frequency

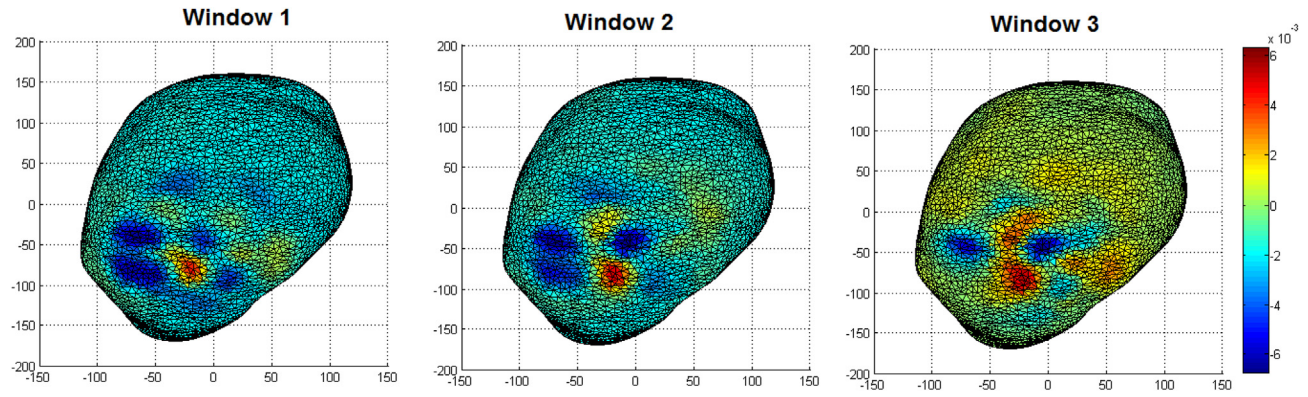


**Fig. 2.** EHG source imaging using SVB-SCCD inverse method of pregnant contraction recorded by 16 electrodes. Windows represent 20 s of averaged data.

content are similar(same activity but delayed). sLORETA generally does not give as accurate results as cMEM. We could not evidence from these preliminary results any kind of linear propagation of the uterine electrical activity as shown also in sheep [47]; rodent [48]; and human [49,50] where the action potentials are not found to travel linearly.

## 5. Conclusion

We can conclude that the STF method cannot properly separate sources when their signals are too correlated. A low correlation between signals of different sources should ease their separation. STWVDA gives less precise results than cMEM for the raw EHG data. Nevertheless, the prewhitening step greatly improves the source localization results obtained by STWVD-DA. The obtained performance is there similar to the one obtained by STWV-DA. When applying SVB-SCCD inverse method to real signals, our analysis of the evolution of the real sources during contraction does not evidence any linear propagation. The activity appears to propagate non linearly and slowly across the muscle with complex pathways and noncontiguously.

## 6. Perspective

In future work we would like to go deeply to the clinical applications (estimating the sizes of the regions, analysing the synchronicity between them). We would also like to improve the model used to solve the forward problem to get a more realistic representation of the uterine behavior. In the ideal, this model should be rendered patient specific to face to the wide interindividual variability encountered in the clinical practice. Indeed, to investigate the performance of this method in localizing synchronous regions from clinical measurements, we have to assume that the electrophysiological model that will be used to constrain the minimization problem is sufficiently accurate.

## Acknowledgement

This research was supported by University of Technology of Compiegne, France and CEDRE.

## References

[1] Abe Y. The hormonal control and the effects of drugs and ions on the electrical and mechanical activity of the uterus. Smooth muscle; 1970. p. 396–417.
[2] Garcia-Casado J, Ye-Lin Y, Prats-Boluda G, Mas-Cabo J, Alberola- Rubio J, Perales A. Electrohysterography in the diagnosis of preterm birth: a review. Physiol Meas 2018;39(2):02TR01.
[3] Fergus P, Cheung P, Hussain A, Al-Jumeily D, Dobbins C, Iram S. Prediction of preterm deliveries from ehg signals using machine learning. PLoS One 2013;8(10):e77154.
[4] Shahrdad M, Amirani MC. Detection of preterm labor by partitioning and clustering the ehg signal. Biomed Signal Process Control 2018;45:109–16.
[5] Devedeux D, Marque C, Mansour S, Germain G, Duchêne J. Uterine electromyography: a critical review. Am J Obstet Gynecol 1993;169(6):1636–53.
[6] Gondry J, Duchêne J, Marque C. First results on uterine emg monitoring during pregnancy vol. 6. 1992. p. 2609–10.
[7] Karlsson B, Terrien J, Gudmundsson V, Steingrimsdottir T, Marque C. Abdominal ehg on a 4 by 4 grid: mapping and presenting the propagation of uterine contractions. 11th Mediterranean conference on Medical and biomedical engineering and computing 2007. Springer; 2007. p. 139–43.
[8] Euliano TY, Marossero D, Nguyen MT, Euliano NR, Principe J, Edwards RK. Spatiotemporal electrohysterography patterns in normal and arrested labor. Am J Obstet Gynecol 2009;200(1):54e1.
[9] Lucovnik M, Maner WL, Chambliss LR, Blumrick R, Balducci J, Novak-Antolic Z, Garfield RE. Noninvasive uterine electromyography for prediction of preterm delivery. Am J Obstet Gynecol 2011;204(3). 228-e1.
[10] de Lau H, Rabotti C, Bijloo R, Rooijakkers MJ, Mischi M, Oei S. Automated conduction velocity analysis in the electrohysterogram for prediction of imminent delivery: a preliminary study. Computational and mathematical methods in medicine 2013;2013:627976. 7 pages.
[11] Horoba K, Jezewski J, Wrobel J, Matonia A, Czabanski R, Jezewski M. Analysis of uterine contractile wave propagation in electrohysterogram for assessing the risk of preterm birth. Journal of Medical Imaging and Health Informatics 2015;5(6):1287–94.
[12] Marque C, Diab A, Laforêt J, Hassan M, Karlsson B. Dynamic behavior of uterine contractions: an approach based on source localization and multiscale modeling. 2015. p. 527–40.
[13] Zahran S, Yochum M, Diab A, Marque C. Variation-based sparse source imaging in localizing uterine activity. Engineering in medicine and biology society (EMBC), 2017 39th annual international conference of the IEEE. IEEE; 2017. p. 2948–51.
[14] Zahran S, Alrifai B, Diab A, Khalil M, Marque C. Separation and localization of ehg sources using tensor models. Advances in biomedical engineering (ICABME), 2017 fourth international conference on. IEEE; 2017. p. 1–4.
[15] Nader N, Zahran S, Marque C, Hassan M, Yochum M, Falou W, Khalil M. Graph analysis of uterine networks using ehg source connectivity. Advances in biomedical engineering (ICABME), 2017 fourth international conference on. IEEE; 2017. p. 1–4.
[16] Zahran S, Diab A, Khalil M, Marque C. Source localization of uterine activity using maximum entropy on the mean approach. 2018 IEEE 4th Middle East conference on biomedical engineering (MECBME). IEEE; 2018. p. 247–51.
[17] Young RC. Myocytes, myometrium, and uterine contractions. Ann N Y Acad Sci 2007;1101(1):72–84.
[18] Caldeyro-barcia R, Poseiro JJ. Physiology of the uterine contraction. Clin Obstet Gynecol 1960;3(2):386–410.
[19] Wolfs GMJA, Van Leeuwen M. Electromyographic observations on the human uterus during labour. Acta Obstet Gynecol Scand 1979;58(sup90):1–61.
[20] Garcia MA, Baffa O. Magnetic fields from skeletal muscles: a valuable physiological measurement? Front Physiol 2015;6.
[21] Lowery, C., Eswaran, H., Murphy, P., Wilson, J., Apr. 9 2003. Uterine magnetomyography. US Patent App. 10/411,027.
[22] Baillet S, Mosher JC, Leahy RM. Electromagnetic brain mapping. IEEE Signal Process Mag 2001;18(6):14–30.
[23] Michel CM, Murray MM, Lantz G, Gonzalez S, Spinelli L, de Peralta RG. Eeg source imaging. Clin Neurophysiol 2004;115(10):2195–222.
[24] Scherg M, Von Cramon D. Evoked dipole source potentials of the human auditory cortex. Electroencephalogr Clin Neurophysiology Evoked Potentials Sect 1986;65(5):344–60.
[25] Koles ZJ. Trends in eeg source localization. Electroencephalogr Clin Neurophysiol 1998;106(2):127–37.
[26] Dale AM, Sereno MI. Improved localizadon of cortical activity by combining eeg and meg with mri cortical surface reconstruction: a linear approach. J Cogn Neurosci 1993;5(2):162–76.
[27] Hämäläinen MS, Ilmoniemi RJ. Interpreting magnetic fields of the brain: minimum norm estimates. Med Biol Eng Comput 1994;32(1):35–42.
[28] Pascual-Marqui RD, Michel CM, Lehmann D. Low resolution electromagnetic tomography: a new method for localizing electrical activity in the brain. Int J Psychophysiol 1994;18(1):49–65.
[29] Trujillo-Barreto NJ, Aubert-Vázquez E, Valdés-Sosa PA. Bayesian model averaging in eeg/meg imaging. NeuroImage 2004;21(4):1300–19.
[30] Clarke C, Janday B. The solution of the biomagnetic inverse problem by maximum statistical entropy. Inverse Probl 1989;5(4):483.
[31] Amblard M. Conventions et comptabilité: vers une approche sociologique du modèle. Comptab Controle Audit 2004;10(3):47–67.
[32] Pascual-Marqui RD, et al. Standardized low-resolution brain electromagnetic tomography (sloreta): technical details. Methods Find Exp Clin Pharmacol 2002;24(Suppl D):5–12.
[33] Chowdhury RA, Lina JM, Kobayashi E, Grova C. Meg source localization of spatially extended generators of epileptic activity: comparing entropic and hierarchical bayesian approaches. PLoS One 2013;8(2):e55969.
[34] Becker H, Albera L, Comon P, Haardt M, Birot G, Wendling F, Gavaret M, Bénar C-G, Merlet I. Eeg extended source localization: tensor-based vs. conventional methods. NeuroImage 2014;96:143–57.
[35] Becker H, Albera L, Comon P, Gribonval R, Merlet I. Fast, variation-based methods for the analysis of extended brain sources. 2014 22nd European signal processing conference (EUSIPCO). IEEE; 2014. p. 41–5.
[36] Kybic J, Clerc M, Abboud T, Faugeras O, Keriven R, Papadopoulo T. A common formalism for the integral formulations of the forward eeg problem. IEEE Trans Med Imaging 2005;24(1):12–28.
[37] Nédélec J-C. Acoustic and electromagnetic equations: integral representations for harmonic problems 144. 2001.
[38] Yochum M, Laforêt J, Marque C. An electro-mechanical multiscale model of uterine pregnancy contraction. Comput Biol Med 2016;77:182–94.
[39] Bibin L, Anquez J, de la Plata Alcalde JP, Boubekeur T, Angelini ED, Bloch I. Whole-body pregnant woman modeling by digital geometry processing with detailed uterofetal unit based on medical images. IEEE (Inst Electr Electron Eng) Trans Biomed Eng 2010;57(10):2346–58.
[40] Gramfort A, Papadopoulo T, Olivi E, Clerc M. Openmeeg: opensource software for quasistatic bioelectromagnetics. Biomed Eng Online 2010;9(1):1.
[41] Miwakeichi F, Martınez-Montes E, Valdés-Sosa PA, Nishiyama N, Mizuhara H, Yamaguchi Y. Decomposing eeg data into space- time-frequency components using parallel factor analysis. NeuroImage 2004;22(3):1035–45.
[42] Becker H, Comon P, Albera L, Haardt M, Merlet I. Multi-way space-time-wave-vector analysis for eeg source separation. Signal Process 2012;92(4):1021–31.
[43] Luciani X, Albera L. Semi-algebraic canonical decomposition of multi-way arrays and joint eigenvalue decomposition. 2011 IEEE international conference on acoustics, speech and signal processing (ICASSP). IEEE; 2011. p. 4104–7.
[44] Luciani. Canonical polyadic decomposition based on joint eigenvalue decomposition. Chemometr Intell Lab Syst 2014;132:152–67.
[45] Grova C, Daunizeau J, Lina J-M, Bénar C, Benali H, Gotman J. Evaluation of eeg localization methods using realistic simulations of interictal spikes. Neuroimage 2006;29(3):734–53.

[46] Cho J-H, Hong SB, Jung Y-J, Kang H-C, Kim HD, Suh M, Jung K-Y, Im C-H. Evaluation of algorithms for intracranial eeg (ieeg) source imaging of extended sources: feasibility of using ieeg source imaging for localizing epileptogenic zones in secondary generalized epilepsy. Brain Topogr 2011;24(2):91–104.
[47] Parkington H, Harding R, Sigger J. Co-ordination of electrical activity in the myometrium of pregnant ewes. J Reprod Fertil 1988;82(2):697–705.
[48] Lammers WJ, Mirghani H, Stephen B, Dhanasekaran S, Wahab A, Al Sultan MA, Abazer F. Patterns of electrical propagation in the intact pregnant Guinea pig uterus. Am J Physiol Regul Integr Comp Physiol 2008;294(3):R919–28.
[49] Rabotti C, Mischi M. Propagation of electrical activity in uterine muscle during pregnancy: a review. Acta Physiol 2015;213(2):406–16.
[50] Diab A, Hassan M, Laforet J, Karlsson B, Marque C. Ehg source localization using signals from a uterus electrophysiological model. Proceedings of virtual physiological human conference. 2014.